CH-95-8-3

A TWO-DIMENSIONAL NUMERICAL MODEL FOR GLAZING SYSTEM THERMAL ANALYSIS

John L. Wright, Ph.D., P.Eng.
Member ASHRAE

Harry F. Sullivan, Ph.D., P.Eng.
Member ASHRAE

ABSTRACT

A simple two-dimensional (2-D) numerical control volume formulation is presented that can be used to model heat transfer through a vertical insulated glazing unit. This model accounts for natural convection of the fill gas (including the effect of secondary cells), conduction within the solid materials, and radiant exchange between the various surfaces facing the fill-gas cavity. This model closely reproduces average and local heat transfer rates measured using a guarded heater plate apparatus. Simulations clearly show that fill-gas motion causes the minimum indoor surface temperature (during cold weather) to be located at the bottom edge of the indoor glazing. Calculated results were also used to gain insights into heat transfer patterns in glazing systems with various combinations of low-emissivity coatings, fill gases, and edge-seal designs.

INTRODUCTION

Windows play a major role in governing the energy consumption of both residential and commercial buildings. They account for a significant portion of the envelope heat transfer and virtually all of the solar gain. As a result, a significant effort has been made to design energy-efficient windows, and the advances made through the implementation of low-emissivity (low-e) coatings and substitute fill gases have transformed the industry.

It is common for sealed, insulated glazing units (IGUs) to exhibit condensation problems when operated in cold climates. Damaging accumulations of water, frost, and ice can form along the perimeter of the exposed surface of the indoor glazing because of the thermal short circuit caused by the edge seal. Condensation most readily forms along the bottom edge of the indoor glazing because this is where the conductive effect of the edge seal is augmented by local cooling caused by fill-gas motion.

The research described here consists of a combination of computer modeling and experimentation. Measurements of heat transfer rates through a variety of glazing systems showed that consistent differences could be found between the heat fluxes occurring near the top and bottom edges of glazing systems. These differences can be explained qualitatively by considering the motion of the fill gas but could only be quantified experimentally. Therefore, the goal of this undertaking was to formulate and test a computer model that accounts for the conduction, radiant exchange, and fill-gas motion within glazing systems. The comparison of calculated and measured results serves not only to validate the model but also demonstrates clearly that fill-gas convection in an IGU causes the minimum indoor glazing temperature to occur at the bottom edge of the glazing. Additional modeling can be used to predict condensation resistance values for windows that are in the design process or undergoing scrutiny for certification.

BACKGROUND

Heat transfer through many glazing systems has been measured using a guarded heater plate apparatus (Wright and Sullivan 1987a, 1987b, 1988). This apparatus consists primarily of two parallel copper plates (each 635 mm by 635 mm by 12.7 mm [25 in. by 25 in. by 0.5 in.]), positioned facing each other, that can be maintained at different but constant temperatures. The warm copper plate contains three guarded heater plates (each 200 mm by 200 mm [7.875 in. by 7.875 in.]) that lie in recesses located in a row across the center of the warm copper plate. They are embedded in such a way that the flat face of each heater plate is flush with the surface of the warm copper. Each heater plate is made of copper. Thus, the warm plate appears to be flat and continuous. It is possible to measure heat transfer that occurs over the face of each guarded heater plate.

IGUs tested in the guarded heater plate apparatus are built to the same face dimensions as the copper plates. Each unit is clamped between the copper plates. In order to promote good thermal contact, sheets of neoprene (rubber) are placed between the IGU and the copper plates. Measurements are usually made with the plates held vertically so that the three measurements of heat flux correspond to areas near the top, middle, and bottom of the IGU.

It was common for tests to be carried out with an interest only in the heat transfer rate measured at the middle heater plate because this provides a good measure of the center-glass U-factor. However, two interesting effects can be seen when the heat transfer rates measured at all three heater

John L. Wright is manager of and a research engineer at the Advanced Glazing System Laboratory and **Harry F. Sullivan** is a professor, both in the Department of Mechanical Engineering at the University of Waterloo, Waterloo, ON, Canada.

plates are examined. First, the heat flux at the top and bottom heater plates was consistently greater than the heat transfer at the middle heater plate. This happens because the low thermal resistance of the edge seals allows more heat transfer at the perimeter of the IGU than in the center-glass area. Second, the heat transfer measured at the bottom heater plate was always greater than the heat transfer at the top heater plate. Gas in the interpane cavity flows upward near the warm glazing and downward near the cold glazing. The descending gas becomes progressively colder. At the bottom of the cavity this cold fill gas turns and comes in direct contact with the bottom of the warm glazing as it starts its ascent. Thus, natural convection of the fill gas increases the heat transfer from the bottom heater plate but not from the top heater plate. It is this medium/low/high progression of heat transfer at the top/middle/bottom heater plates that was expected in results obtained from the numerical simulation of an IGU installed in the guarded heater plate apparatus.

THE COMPUTATIONAL MODEL

In order to enable a direct comparison between calculated and measured average and local heat transfer rates, a 2-D model was configured to simulate a glazing system under the conditions of a guarded heater plate test. Details of the problem domain and pertinent nomenclature are shown in Figure 1. The glazings are separated from the isothermal boundaries (i.e., the copper plates) by two sheets of neoprene rubber and the top and bottom ends of the problem domain are assumed to be adiabatic.

The glazing system model was developed by extending an existing and proven model (Wright 1990; Wright and Sullivan 1994) for natural convection of gas in a tall, vertical, rectangular cavity. The natural convection model was extended to solve for the temperature and heat flux distributions in double-pane glazing system assemblies. Modifications required to model this composite problem domain involved the additional consideration of conductive heat transfer in the solid sections (i.e., glazings and edge seals) and the exchange of energy by thermal radiation between the surfaces exposed to the interpane cavity. The following subsections describe the convection, conduction, and radiant exchange models. The description of the natural convection model is brief because detailed documentation can be found in the literature (Wright and Sullivan 1994).

Fill-Gas Convection

The natural convection model consists of a numerical (control volume) solution of the differential equations that describe the conservation of energy, horizontal and vertical momentum, and mass. The numerical algorithm used to solve these four equations, called SIMPLEC (Vandoormaal and Raithby 1984), is an extension of the semi-implicit method for pressure-linked equations (SIMPLE), described by Patankar (1980). SIMPLEC consists of an iterative "coefficient update loop" within which each of the four required conservation equations is solved in sequence. The only extension to the SIMPLEC procedure was the additive correction method (ACM) of Hutchinson and Raithby (1986), which was used to speed convergence.

The velocity and heat transfer solutions for fill-gas flow in a vertical window cavity are determined largely by the Rayleigh number (Ra). In the case of a fixed-pane spacing and a specified fill-gas composition, Ra is proportional to the temperature difference between the cavity walls. Ra typically does not exceed 12,000 under severe winter conditions in windows designed with optimum pane spacing. Various research studies have shown that in addition to the primary or base flow of fill gas that exists at low Ra, a stationary "cat's eye" pattern of secondary cells can be expected in the core of the flow when Ra exceeds a critical value (Wright and Sullivan 1989a). Bergholtz (1978) provided a means by which this critical Rayleigh number could be easily calculated and showed that cells can be expected for Ra > 5,600 in tall window cavities. The natural convection model used in this study incorporates a unique flow perturbation scheme that induces secondary cells when Ra is sufficiently high (Wright 1990; Wright and Sullivan 1994).

Solid Sections

The solid sections included in the problem domain consist of two sheets of neoprene, two sheets of glass, and two edge seals. Each of these three solids was treated as a homogeneous material.

The control volume arrangement was laid out to incorporate the glazing system materials and neoprene mats. The x-direction index, i, begins and ends at $i = ib$ and $i = ie$, respectively. The ib and ie control volumes correspond to the layers of neoprene. The glazings are located at $i = ib + 1$ and $i = ie - 1$. The cavity includes control volumes from $i = ibc = ib + 2$ to $i = iec = ie - 2$. The edge seals are uniformly split into the same number of horizontal divisions as the interpane cavity (i.e., 25 columns of control volumes). The grid aspect ratio in the cavity was set at $A_{grid} = 5$ and the same vertical subdivision used in the cavity was used for the glazing and neoprene materials adjacent to the cavity. The edge seals were divided into n_{seal} vertical divisions such that the size of the seal control volumes was about the same as that of the cavity control volumes (usually $n_{seal} = 5$). The same vertical divisions were used to set up control volumes in the glazings and neoprene adjacent to the edge seals. The y-direction index, j, runs from $j = jb$ to $j = je$ over the entire problem domain and from $je = jbc$ to $j = jec$ over the height of the cavity.

Some of the glazing systems tested contained edge seals built up from more than one component (i.e., spacer, sealants, etc.). The simulation model treated the edge seal as a single, homogeneous material. In order to be realistic, the thermal conductivity assigned to the fictitious seal material,

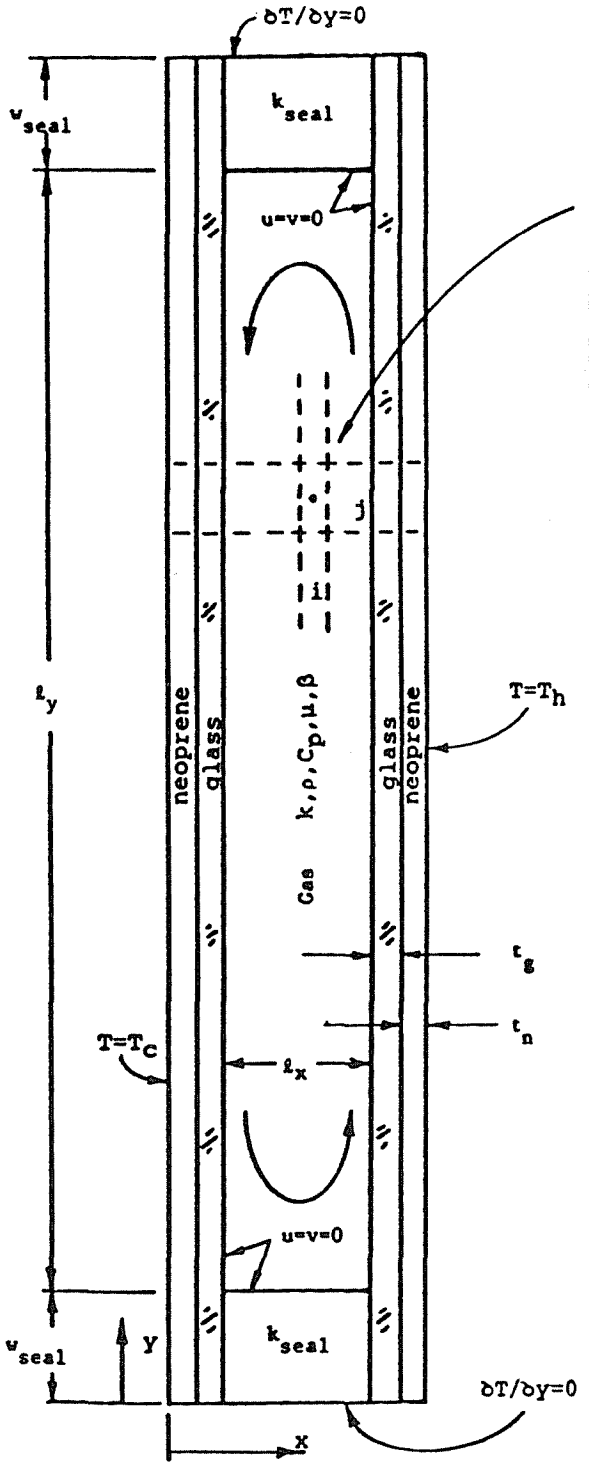

Figure 1 *Two-dimensional glazing system thermal analysis geometry.*

k_{seal}, was based on thermal resistance measurements made using edge-seal samples tested in the guarded heater plate apparatus (Wright and Sullivan 1989b; Wright 1989, 1990).

The solution procedure used to model the composite problem was not complicated. One unique detail concerned the way in which the boundary conditions were applied. The energy balance was applied over the entire problem domain, with the thermal boundary conditions (see Figure 1) applied at the outer edges. This step in the coefficient update loop generated a temperature solution for all control volumes. However, the velocity boundary conditions, used in solving balances to conserve momentum and mass, were applied at the walls of the cavity. Thus, the natural convection velocity field in the cavity was generated for nonuniform temperature distributions at the cavity walls and all velocities at locations outside the cavity were set to zero.

Application of the energy balance across the composite problem domain required care to ensure that the heat flux was correctly calculated at surfaces between materials of different thermal conductivity. Fortunately, such surfaces only exist where the velocity is zero; in these locations, bookkeeping is only required to keep track of heat transfer by conduction. The conductive heat flux at such control volume faces was calculated according to the procedure outlined by Patankar (1980). For example, at a surface on the west wall of the interpane cavity (as shown in Figure 2), the surface temperature, T_{surf}, is given by

$$T_{surf} = \frac{T_{ibc-1,j}\frac{k_g}{t_g} + T_{ibc,j}\frac{k}{\Delta x}}{\frac{k_g}{t_g} + \frac{k}{\Delta x}} \quad (1)$$

where t_g and Δx are the thicknesses of the glass and the fill-gas control volume adjacent to the glass surface, respectively, and k_g and k are the conductivities of the glass and fill gas, respectively. The corresponding surface heat flux, q_{surf}, is given by

$$q_{surf} = 2\frac{k_g}{t_g}(T_{ibc-1,j} - T_{surf}) = 2\frac{k}{\Delta x}(T_{surf} - T_{ibc,j}). \quad (2)$$

THERMAL RADIATION MODEL

Figure 1 shows the fill-gas cavity. Each of the four cavity walls can be divided into finite surfaces—each of which emits, reflects, and absorbs thermal radiation. The incident radiative flux (or irradiance) at the pth surface is denoted H_p and can be expressed as

$$H_p = \frac{1}{A_p}\sum_{vnb} A_{nb}E_{nb-p}B_{nb} \quad (3)$$

where the summation is carried out for all of the "visible neighbor" wall surfaces (i.e., for all surfaces from which radiation can reach surface p). A_{nb} is the surface area of a

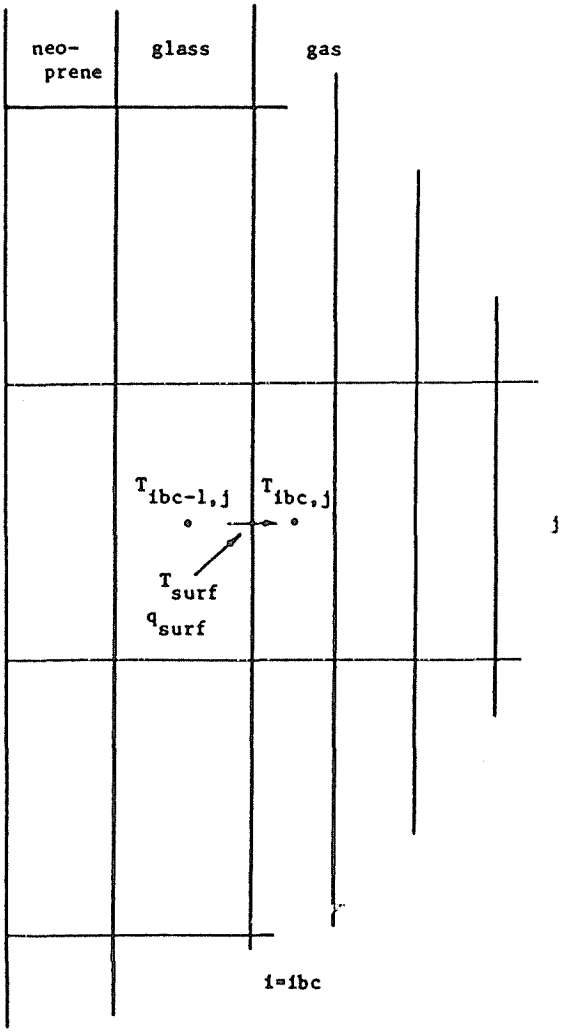

Figure 2 *Surface heat flux and temperature at the cavity wall.*

neighbor surface, E_{nb-p} is the geometric exchange factor from a neighbor surface to surface p, and B_{nb} is the radiative flux leaving (i.e., the radiosity at) the neighbor surface. Using the reciprocity relation,

$$A_{nb}E_{nb-p} = A_pE_{p-nb}, \tag{4}$$

Equation 3 can be simplified:

$$H_p = \sum_{vnb} E_{p-nb}B_{nb}. \tag{5}$$

If all surfaces are treated as diffusely emitting and reflecting, then the exchange factors, E_{p-nb}, are equal to the more familiar geometric radiative shape factors, F_{p-nb}. However, it was thought possible that an appreciable portion of the radiation reflected from a glass surface would be reflected in a specular manner—especially if a low-e coating were present. It has been shown that subdivision of the hemispheric reflectance into specular and diffuse components, coupled with the assumption of diffuse emission, lends itself to analytical treatment (Sparrow and Cess 1976). In accordance with this method, the reflectances of the vertical walls were split into specular and diffuse components as shown in Equation 6:

$$\rho = 1-\varepsilon = \rho^s + \rho^d. \tag{6}$$

Using this formulation for reflectance, B_{nb} can be expressed as the sum of emitted flux (surface temperature = $T_{surf,nb}$) and the diffusely reflected portion of the irradiance:

$$B_{nb} = \varepsilon_{nb}\sigma T^4_{surf,nb} + \rho^d_{nb}H_{nb}. \tag{7}$$

By combining Equations 5 and 7 and rearranging, one obtains the following:

$$H_p - \sum_{vnb} E_{p-nb}\rho^d_{nb}H_{nb} = \sum_{vnb} E_{p-nb}\varepsilon_{nb}\sigma T^4_{surf,nb}. \tag{8}$$

Equation 8 can be expressed, for all surfaces of the cavity, in matrix format:

$$[A]\,[H] = [T] \tag{9}$$

where the transpose of $[H]$ is given by

$$[H]^t = (H_1, H_2, H_3, \ldots) \tag{10}$$

and the entries of the pth row of the coefficient matrix, $[A]$, are given by the left-hand side of Equation 8. The pth entry of the column vector, $[T]$, is given by the right-hand side of Equation 8. The solution to Equation 10 can be expressed in terms of the inverse of $[A]$:

$$[H] = [A]^{-1}[T]. \tag{11}$$

Notice that $[A]$ is a function of optical properties and geometry but does not depend on surface temperatures. It needs to be solved only once for a given cavity and selected set of surfaces. (In fact, the computer code does not invert the $[A]$ matrix, but reaches the same end by calculating its LU decomposition. Details can be found in chapter 2 of Press et al. [1986].) The $[T]$ vector is a function of the surface temperatures. Therefore, for a given distribution of surface temperatures, $[T]$ can be generated and the solution for $[H]$ using Equation 11 requires little computer time.

The exchange factors, E_{p-nb}, also need only be calculated once for a given geometry. Significant simplification in the calculation of E_{p-nb} follows from the fact that ρ^s is constant over all of the individual surface subdivisions that comprise each of the walls and from the assumption that ρ^s can be set to zero for the horizontal walls. Consider the calculation required if surface p is on the west wall of the cavity and the neighbor surface being considered is on the opposite wall. Figure 3 shows this geometry. It can be seen that E_{p-nb} is

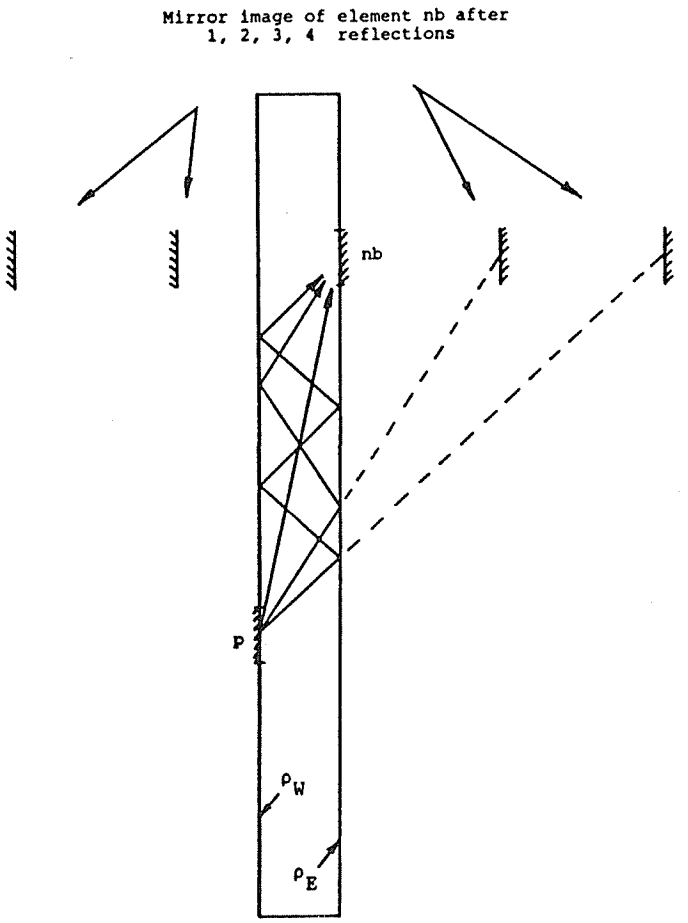

Figure 3 *Example of geometry for calculation of E_{p-nb} radiative exchange factor.*

$$E_{p-nb} = F_{p-nb} + \sum_{i=1}^{\infty} (\rho_W^s)^i (\rho_E^s)^i F(2i)_{p-nb} \qquad (12)$$

where ρ_W^s and ρ_E^s are the specular reflectance values for the west and east vertical walls, respectively. $F(2i)_{p-nb}$ is the geometric shape factor from surface p to the mirror image of surface nb after $2i$ reflections in the vertical walls. Each F_{p-nb} was computed using Hottel's crossed-string rule (Siegel and Howell 1972), and Equation 12 (or one of several similar equations) was applied by including the first 100 terms in the summation. Knowing that all radiation leaving any surface must eventually be absorbed or diffusely reflected at some surface, the accuracy of the calculated exchange factors was verified using the following check-sum:

$$\sum_{\forall nb} E_{p-nb}(1-\rho_{nb}^s) = 1 \qquad (13)$$

for any surface, p.

If the fill-gas cavity is bounded by n gray surfaces on each vertical wall and m surfaces on each horizontal wall and their temperatures are taken as being fixed, then the application of Equation 8 at each surface requires the solution of $2(n+m)$ simultaneous equations—yielding $2(n+m)$ values of H_p. This procedure also entails the calculation and storage of $2(n+m)^2$ values of E_{p-nb}. It was recognized that the computing requirements would be unnecessarily excessive if the surfaces specified for the radiation solution directly matched the control volume grid used for the convection and conduction portions of the analysis (i.e., $n \approx 250$, $m \approx 25$) .

Fortunately, there is a large section away from the ends of the cavity (the center-glass section) where the temperatures of the vertical walls were expected to be isothermal. It was assumed that the center-glass portion of each glazing could be treated as a single surface for the purpose of applying Equation 8. These large center-glass surfaces were delimited according to the ASHRAE definition of center-glass area—exposed faces of finite control volumes starting more than 65 mm from the sight line were included in the center-glass surface. In the edge-glass portions of the cavity, the individual exposed faces of the control volumes were used in the analysis of radiation exchange. This approach reduced the number of H_p variables by a factor of about 4 and reduced the required storage for E_{p-nb} by a factor of more than 10.

Once the irradiance at each enclosure surface was known, the net flux of radiant energy into the surface, S_p, could be found:

$$S_p = \varepsilon_p (H_p - \sigma T_{surf,p}^4) . \qquad (14)$$

S_p was included as a fixed energy source in the energy balance of the wall control volumes. The rate of energy generation per unit volume, S, at any wall control volume is

$$S = \frac{S_p}{\Delta n} \qquad (15)$$

where Δn is the dimension of the control volume normal to the wall. The validity of the source terms was examined during each simulation by summing energy generation at the cavity wall control volumes. This total should be zero. S_p and S were updated at each iteration of the coefficient loop after the generation of a new temperature field.

SOLUTION CONVERGENCE

The 2-D glazing system simulation software was coded in a Fortran program called IGU-2D (Wright 1990). The SIMPLEC algorithm used to generate a numerical solutionis iterative in nature and the criterion for solution convergence in this case was based on the calculation of total heat transfer through the glazing system, Q. The IGU was subdivided into 29 columns of control volumes. Therefore, it was possible to calculate Q at 30 vertical cuts in the problem domain. Once the converged solution has been reached, these estimates of Q should be equal because adiabatic surfaces were pre-

scribed at the top and bottom boundaries. Q was calculated at the right-hand edge of the ith column of control volumes using

$$Q = Q_{rad} + \sum_{j=jb}^{je} q_{i,j}\Delta y_j \tag{16}$$

where

Q_{rad} = net amount of thermal radiation energy crossing the vertical cut from right to left (it can be determined by summing the rate of energy generation due to source terms at wall control volumes to the left of the vertical cut) and

$q_{i,j}$ = nonradiative, right-to-left heat flux through the right-hand face of the (i,j)th control volume. This heat flux, for vertical control volume faces within the cavity, is given by

$$q_{i,j} = \beta\frac{(T_{i+1,j} - T_{i,j})}{\Delta x}k - \rho C_p u_{i,j}\left\{\left(\frac{1}{2}+\alpha\right)T_{i,j} + \left(\frac{1}{2}-\alpha\right)T_{i+1,j}\right\}. \tag{17}$$

Note that α and β are upwinding coefficients calculated as a function of local fluid velocities for the purpose of evaluating the temperature and temperature gradient of the fill gas at each of the control volume faces. A good discussion of upwinding coefficients can be found in Patankar (1980) and details of how they were used in this particular study can be found in Wright (1990) and Wright and Sullivan (1994). In the case of control volume faces along the cavity walls, $q_{i,j}$ was calculated according to Equation 2.

During each execution of IGU-2D, the rate of heat transfer was calculated at the 30 vertical cuts and the maximum and minimum of these values, Q_{max} and Q_{min}, respectively, were noted. Iteration of the coefficient update loop was terminated when Q_{max} and Q_{min} differed by less than 0.1%.

PRELIMINARY RESULTS

Four preliminary simulation runs were carried out in order to examine the sensitivity of the solution to the specular/diffuse split chosen for the longwave reflectivities of the vertical cavity surfaces. Two glazing systems were modeled: a conventional double-glazed unit and a similar unit with a soft, low-e coating. Both glazing units had corrugated-strip edge seals and the fill gas was air. Two simulations were run for each glazing system. Highly specular reflectance properties were used in one simulation and purely diffuse reflectances were used in the other. In the specular runs, the glass surfaces were modeled with $\rho^s = 0.15$ and $\rho^d = 0.01$; the low-e surfaces were modeled with $\rho^s = 0.90$ and $\rho^d = 0.01$. In the diffuse runs, the glass surfaces were modeled with $\rho^s = 0.0$ and $\rho^d = 0.16$; the low-e surfaces were modeled with $\rho^s = 0.0$ and $\rho^d = 0.91$.

The output from each pair of simulations showed very little or no difference in all reported quantities. For example, the local heat fluxes calculated for the areas corresponding to the locations of the guarded heater plates differed at most in the fourth significant digit. Plotted heat flux and temperature profiles appeared to be identical. It was concluded that the diffuse/specular longwave reflection split at the glazing cavity surfaces has no significant bearing on heat transfer in glazing units. All surfaces were subsequently modeled as purely diffuse reflectors.

COMPARISON WITH MEASURED HEAT FLUX

Seven glazing systems were tested using the guarded heater plate apparatus and modeled using IGU-2D. All except one had low-e coatings. Two units had argon fill gas. The set of edge seals incorporated in the test units was purposely chosen to span a wide range of thermal resistance. They included the highly conductive conventional (aluminum spacer bar) edge seals, corrugated-strip edge seals[1] with intermediate thermal resistance, and spacers made from strips of rigid insulating foam. The various data needed to describe the glazing systems are listed in Table 1.

In order to simulate glazing systems installed in the guarded heater plate apparatus, the top and bottom edges of each glazing system were treated as adiabatic surfaces. When measurements were undertaken, these same surfaces were well insulated and it was assumed that any heat flux through the ends of the glazing system would be very small in relation to the heat flux between the glazings through the edge seals. Thus, measurement errors due to the nonadiabatic end condition were assumed to be negligible. However, this may not have been the case for measurements taken when highly insulating foam spacers were used. The same foam that was used for edge spacers was also used to insulate the edge of the test section. Therefore, even though the possibility of a calculation/measurement mismatch was foreseen, it was decided that the foam spacers should be simulated because of the insight to be gained by examining the heat flux patterns in systems with highly insulated edge seals and because of the chance that the nonadiabatic experimental boundary condition was unimportant or that its impact might be quantified.

Figure 4 shows a sample solution (glazing unit 3) of heat flux at the right-hand edge of the problem domain (i.e., at the vertical surface where $T = T_h$). This surface corresponds to the face of the hot copper plate in the guarded heater plate apparatus. The heat flux from the hot copper plate is shown as a function of distance from the bottom of the glazing unit. Glazing unit 3 was built with conventional edge seals that contain aluminum spacer bars. Figure 4 shows that the low thermal resistance of this edge seal results

[1]This is a commercially available edge seal consisting of a corrugated aluminum spacer strip embedded in a strip of sealant.

TABLE 1
Calculated and Measured Glazing System Heat Flux Results

	ΔT_{pp} [°C]	l_x [mm]	w_{seal} [mm]	k_{seal} [W/m·K]	t_n [mm]	t_g [mm]	ε_{le}	ε_{seal}	q_{meas} [W/m^2] Top/Middle/Bottom	q_{calc} [W/m^2] Top/Middle/Bottom
1)	18.88	12.13	9.53	0.52	3.175	3.94		0.827	96.9	90.1
									95.3	89.4
	fill gas air, no coatings								105.7	96.7
2)	19.39	12.41	9.53	0.53	3.175	2.84	0.096	0.827	49.0	45.1
									47.0	44.1
	fill gas air								58.9	55.0
3)	19.12	14.12	11.05	2.56	1.524	3.3	0.047	0.054	32.1	33.5
									28.7	28.0
	fill gas argon								45.7	45.6
4)	11.38	11.96	11.3	2.12	3.175	3.91	0.094	0.054	24.4	24.5
									19.7	19.9
	fill gas argon								27.67	27.1
5)	27.42	16.0	25.4	0.035	1.524	5.59	0.07	0.579	56.5	44.9
									62.7	56.1
	fill gas air								89.0	87.2
6)	27.34	13.0	25.4	0.035	1.524	5.59	0.07	0.579	60.8	50.2
									61.2	59.6
	fill gas air								83.7	82.6
7)	14.86	13.0	25.4	0.035	1.524	5.59	0.07	0.579	32.3	26.6
									30.6	30.2
	fill gas air								38.7	38.7

Notes:
1) Calibration of neoprene mats: k_n=0.17 W/m·K for 1.524 mm mats and k_n=0.19 W/m·K for 3.175 mm mats.
2) k_{seal} was based on seal dimensions and measured linear conductance, k_{lin}, values found in Wright and Sullivan (1989b). k_{lin}=0.41 W/m·K (corrugated strip seals) for units 1 and 2; k_{lin}=2.0 W/m·K (conventional seals) for units 3 and 4. Units 5, 6 and 7 had rigid insulating foam spacers without sealant and k_{seal}=0.035 W/m·K was taken directly from the manufacturer's literature.
3) Emissivities of seals, ε_{seal}, and low-e coatings, ε_{le}, were measured using a Gier-Dunkel DB-100 Infrared Reflectometer.

in a very high heat flux (in excess of 600 W/m^2) near the top and bottom edges of the glazing unit. Heat flux through the center-glass area is constant except for the small variation caused by the secondary cells. The asymmetry between the top and bottom edge-glass areas is a result of the fill-gas motion.

Figure 4 also shows three average values of the calculated heat flux corresponding to the locations of the guarded heater plates where heat transfer was experimentally metered. These results can be directly compared to measured heat flux results. The medium/low/high progression of heat flux found at the top/middle/bottom heater plates is typical of measured values taken for many glazing units tested using the guarded heater plate apparatus. The middle heater plate area provides a representative measure of center-glass heat flux. The heat flux from the top and bottom heater plates is augmented by the thermal short circuit at the edge seal, and the motion of the fill gas further increases the heat flux from the bottom heater plate.

Two sets of heater-plate-area heat flux results are included in Table 1 for each glazing system—one set calculated and one set measured. Each set consists of heat flux data for the top, middle, and bottom heater plates. The same results are presented in bar-chart format in Figure 5.

Units 1 and 2

The first two glazing units for which results are shown in Figure 5 were built using corrugated-strip edge seals. The fill gas was air. Unit 1 had no coatings but unit 2 had a soft,

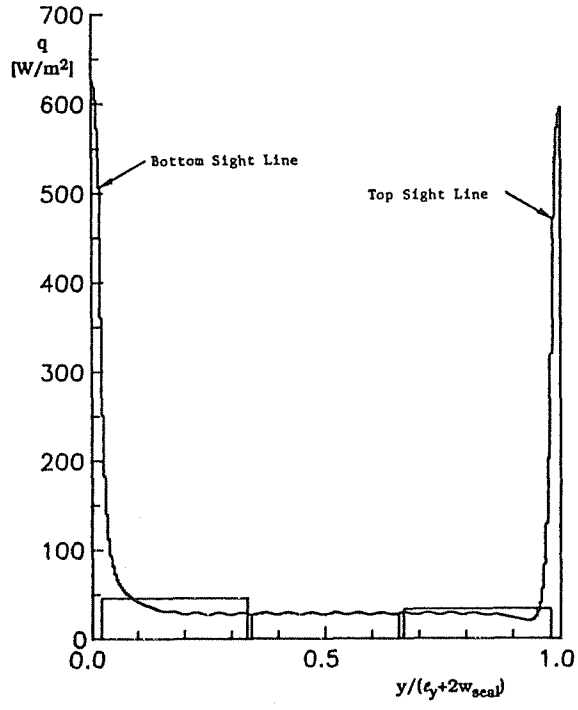

Figure 4 *Calculated heat flux distribution at hot boundary and calculated average heat flux for heater plate areas (unit 3).*

low-e coating. Secondary cells were not expected and were not modeled for either of these glazing units. These units were tested at about the same temperature difference but unit 2 allowed about half as much heat transfer as unit 1 because of the low-e coating. The difference between heat flux at the center and bottom heater plates was greater for unit 2 because the low-e coating suppresses center-glass heat transfer but does not alter the thermal resistance of the edge seals.

The calculated heat flux results consistently underpredicted the measured data from units 1 and 2 by about 7%. This level of discrepancy is not unreasonable but the fact that it exists for both units and is independent of heater plate location suggests that improvement might be possible if the reason(s) for the difference were known. In addition to showing good agreement with the measured heat flux data, the trend in the calculated results closely follows the top/middle/bottom heater plate trend that was found in the measurements.

Units 3 and 4

Glazing units 3 and 4 were both built with conventional, aluminum spacer bar edge seals and both contained argon fill-gas. Unit 4 had a conventional soft, low-e coating. Unit 3 had a more recently developed soft, low-e coating with extremely low emissivity. Secondary cells were modeled in unit 3 but not in unit 4, which was tested at a lower temperature difference.

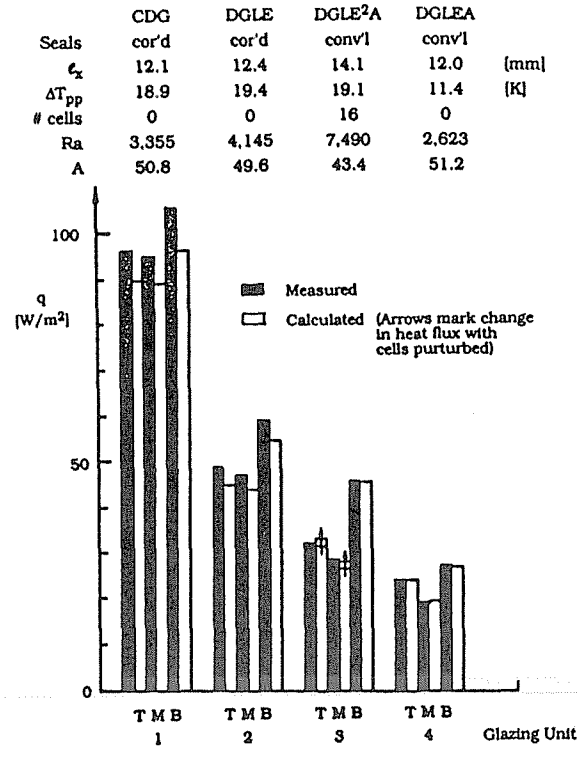

Figure 5a *Calculated and measured heat flux results for top, middle, and bottom guarded heater plate areas (units 1, 2, 3, and 4).*

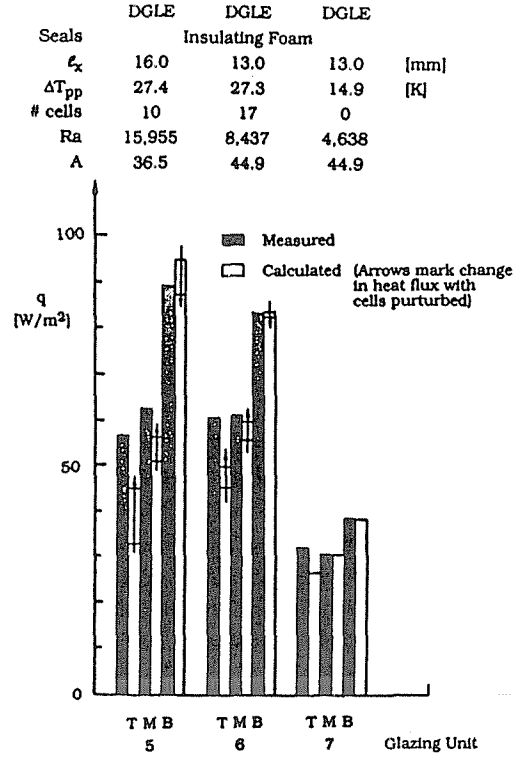

Figure 5b *Calculated and measured heat flux results for top, middle, and bottom guarded heater plate areas (units 5, 6, and 7).*

The agreement between calculated and measured heat flux in these glazing units was excellent. The heater plate heat flux was predicted to within 2% in five of the six cases. Arrows marked in Figure 5 indicate the difference in calculated heat flux resulting from the presence of secondary cells. The results for unit 3 show that Ra was low enough so that the secondary cells had little impact on the heat flux. The presence of cells augmented the heat flux at the top and middle heater plates by about 4% but caused little change (a very slight decrease) at the bottom heater plate.

Again, the customary top/middle/bottom trend in heat flux was observed because of the highly conductive edge seals. Note that the bottom heater plate heat flux was about 50% higher than the heat flux at the middle heater plate for units 3 and 4. The corresponding difference for units 1 and 2 was only about 25% because they were built with the less conductive corrugated-strip edge seals.

Unit 3 was tested with about the same temperature difference used to test units 1 and 2. By examining the heat flux at the center heater plate, it can be seen that the thermal resistance at the center of the test section was approximately doubled by the addition of the low-e coating. The subsequent use of argon fill-gas almost doubled the thermal resistance again.

Units 5, 6, and 7

Test units 5, 6, and 7 each contained a soft, low-e coating and had air as the fill gas. These three units did not incorporate commercial edge seals. Instead, the glazings were separated at their edges by strips of rigid, insulating foam. No sealant was used. Thus, the edge seal consisted of a single material with an extremely low thermal conductivity.

Units 5, 6, and 7 do not exhibit the top/middle/bottom trend in heat flux usually found in glazing systems because the low-conductivity spacers do not drive the heat flux up drastically at the top and bottom. Consequently, the heat flux at the top heater plate is about the same as, or may even be less than, the heat flux at the middle heater plate. It is interesting that the creation of cells in units 5 and 6 decreased the heat flux at the bottom heater plate.

The calculated and measured heat fluxes for unit 5 do not agree as well as the results for any of the other units. The heat flux measured at the center heater plate was 23% higher than the heat flux calculated without secondary cells. This discrepancy was cut in half after cells were introduced. The reason for the disparity can be understood by noting that the relatively large pane spacing and high temperature difference resulted in Ra being well in excess of the range of Ra for which the convection model was intended ($Ra \approx 16,000$, based on center-glass temperature difference across the cavity). On the basis of results shown in Wright and Sullivan (1994), it can be seen that the numerical convection model would underpredict the heat transfer rate by almost 20% at Ra = 16,000 if no cells were present and that only half of the difference would be made up if cells were induced.

The simulation results for units 6 and 7 closely match the measured heat fluxes for the bottom and middle heater plates. In these locations, discrepancies were 3% or less. In contrast, the heat flux at the top heater plate was underpredicted by 21% in both units 6 and 7. Notice that the top heat flux was also underpredicted by about 25% for unit 5. This difficulty in calculating heat flux at the top heater plate exists only for units 5, 6, and 7—the units with highly insulating edge spacers. The specific reason for this is not clear but it is likely that this problem is linked to the adiabatic boundary assumption. Fortunately, the model does not exhibit the same difficulty when more conventional edge seals are used or at the bottom of the glazing system, where the heat flux and temperature profiles are of greatest interest.

HEAT FLUX IN THE GLAZING CAVITY

Having completed the comparison of calculated and measured heat fluxes at the problem boundary it is instructive to study the simulation results for details about heat flux within the glazing unit itself. Test units 1, 2, 3, and 7 were chosen for examination because they include glazing systems with and without a low-e coating, with and without argon fill-gas, and all three variations in edge-seal conductance. Units 1, 2, and 3 were tested at approximately the same temperature difference, facilitating the comparison of heat flux results. The simulation results for units 1, 2, 3, and 7 were assumed to be accurate on the basis of the comparisons presented in the previous section.

Figures 6, 7, 8, and 9 show the local x-direction heat flux, $q(y)$, plotted as a function of distance from the bottom of the glazing system for a vertical surface located at the hot wall of the cavity (i.e., $x = t_n + t_g + l_x$). Figures 6 through 9 show results for test units 1, 2, 3, and 7, respectively. Each figure includes two curves, with the higher curve showing total heat flux and the lower curve showing the radiative component. The hash marks on the lower curve delimit the center-glass portion of the glazing system as specified in the analysis of radiative exchange, which in all cases corresponds to the center-glass area defined by ASHRAE. The sight lines are located where the radiative heat flux becomes zero and the total heat flux rises sharply.

Figure 6 shows heat flux results for a conventional double-glazed IGU with corrugated-strip edge seals (unit 1). The heat flux is constant over the center-glass area, and radiative exchange constitutes the majority of the center-glass heat transfer. In the bottom edge-glass area, the heat flux increases because of the fill-gas motion. Heat flux through the edge seals peaks at more than 400 W/m^2 and is significantly higher than the heat flux through any portion of the sight area.

Unit 2 was similar to unit 1 except that a low-e coating was included in unit 2. These two units can be compared by

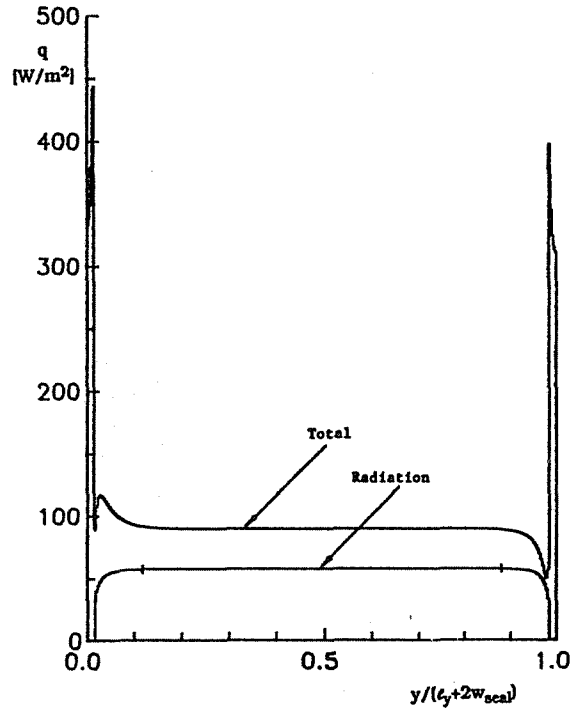

Figure 6 *Heat flux component distributions along vertical cut at hot cavity wall (unit 1).*

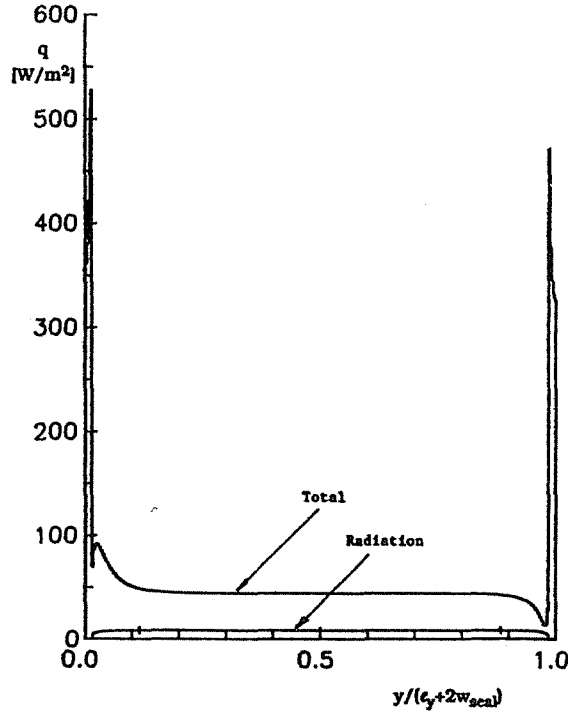

Figure 7 *Heat flux component distributions along vertical cut at hot cavity wall (unit 2).*

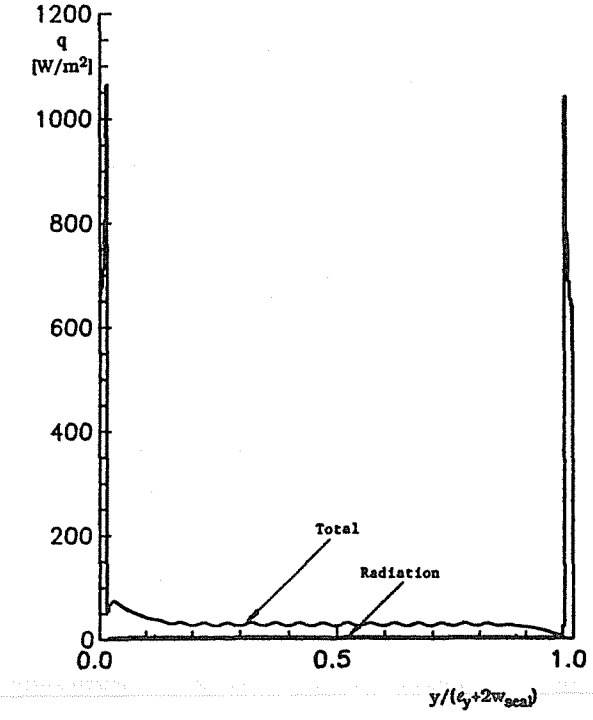

Figure 8 *Heat flux component distributions along vertical cut at hot cavity wall (unit 3).*

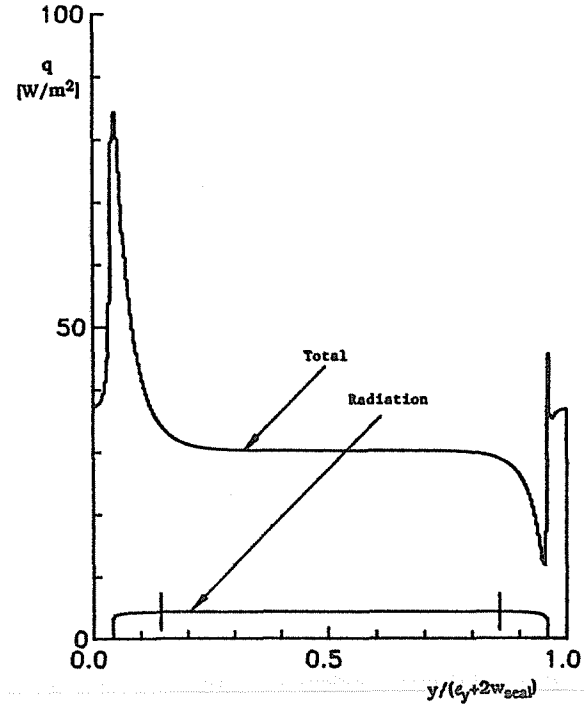

Figure 9 *Heat flux component distributions along vertical cut at hot cavity wall (unit 7).*

examining Figures 6 and 7. The pattern of heat flux is similar for units 1 and 2 but the total center-glass and edge-glass heat flux has been substantially reduced because the low-e coating has virtually eliminated the radiative heat flux in unit 2. In contrast, the peak edge-seal heat flux is greater in unit 2 (in excess of 500 W/m^2) than it was in unit 1. It is interesting that the increased edge-seal heat flux results from the presence of the low-e coating. The increase in edge-glass and center-glass thermal resistance imposes a larger temperature difference across the edge seals.

Units 2 and 3 can be compared by examining the results in Figures 7 and 8. The differences between these units include a switch from corrugated-strip to conventional edge seals and the presence of argon fill-gas instead of air. Again, the low-e coating limits the radiative heat flux to a small portion of the total. The secondary cells in unit 3 create a ripple in the heat flux distribution. The use of argon in unit 3 has reduced the center-glass and edge-glass heat flux. The use of conventional edge seals and the relatively high thermal resistance of the sight area have caused the peak heat flux in the edge seals to be in excess of 1,000 W/m^2.

Figure 9 shows heat flux results for unit 7. Unit 7 was similar to unit 2 except for the use of insulating foam instead of the corrugated-strip edge seals. Unit 7 was tested at a lower temperature difference (ΔT_{pp} = 14.9°C versus 19.4°C). The center-glass thermal resistance of unit 7 was approximately the same as that for unit 2. The effect of the insulating foam spacer used in unit 7 is apparent in that the peak heat flux did not exceed 90 W/m^2, which is an order of magnitude less than the peak heat flux found in unit 3. Away from the cavity wall, the edge-seal heat flux drops to almost the level of the center-glass heat flux. The asymmetry of the heat flux distribution caused by the fill-gas motion is highly pronounced in the results shown for unit 7.

Several observations can be made regarding results that are common to Figures 6 through 9. In each case the radiant heat flux distribution did not show a discontinuity at the junction of the edge-glass and center-glass areas. This result supports the validity of lumping the center-glass control volume surfaces together for the purpose of the radiative exchange model. The simulations also seem to give credence to the ASHRAE definition of center-glass area in that heat flux results were very close to being constant within the center-glass limits, but this may be misleading because of the isothermal boundary conditions imposed by the guarded heater plate apparatus. In all cases, the heat flux profiles were asymmetric, with the natural convection of the fill gas causing the bottom edge-glass heat flux to be significantly greater than the center-glass or top edge-glass heat flux. This asymmetry is most evident in units with highly insulating edge seals. This augmentation of heat flux at the bottom edge of the sight area corresponds to the location of the minimum indoor glazing temperature where the onset of condensation occurs during cold weather.

TEMPERATURE PROFILES AT THE WARM GLAZING

Temperature profiles, $T(y)$ versus y, have been produced for a plane at the hot vertical wall of the glazing cavity. This surface is the same vertical cut at which heat flux profiles were given in Figures 6 through 9. Figures 10 through 13 show temperature profiles for units 1, 2, 3, and 7 that correspond to Figures 6 through 9, respectively.

Figures 10, 11, and 12 show that the center-glass temperature drew progressively closer to the hot plate temperature as the center-glass thermal resistance of the glazing system increased. The same effect is apparent in windows exposed to the environment. Glazing systems with higher thermal resistance exhibit higher indoor glazing temperatures in cold weather and are less susceptible to condensation.

The location of the minimum indoor pane temperature is at (or very near) the bottom sight line. The extreme edges of the indoor glazing may exist at a lower temperature, but the glass outside the sight line is generally not exposed to the indoor air after being installed in a sash. Condensation forms first at the bottom sight line. The sight line temperature predictions resulting from simulation of the guarded heater plate configuration offer no quantitative information regarding windows exposed to more realistic conditions, but qualitative observations can be made.

Examining Figures 9 through 13, the minimum temperature at the bottom sight line was consistently lower than the temperature at the top sight line. This difference would not have been evident if the motion of the fill gas had not been modeled. The difference between the top and bottom sight line temperatures was less than 1°C in all four cases. This difference would be greater if the glazing system were exposed to the indoor environment rather than being held close to an isothermal plate.

In the three units constructed with commercial edge seals (see Figures 10, 11, and 12) the temperature of the warm glazing continued to drop along the edge seal below the bottom sight line. This is consistent with the heat flux profiles shown in Figures 6, 7, and 8, where the heat flux also was also found to decrease across the face of the edge seal. Only in the glazing system with insulating foam spacers (shown in Figure 13) was an increase in temperature found below the bottom sight line.

CONCLUSIONS

A model has been formulated for the numerical simulation of heat transfer in glazing systems. This model includes the 2-D treatment of glazing and edge-seal conduction, the exchange of thermal radiation between the glazings, and natural convection of the fill gas (including secondary cells if needed). Simulation results pertain to both the center-glass and edge-glass areas of the glazing system.

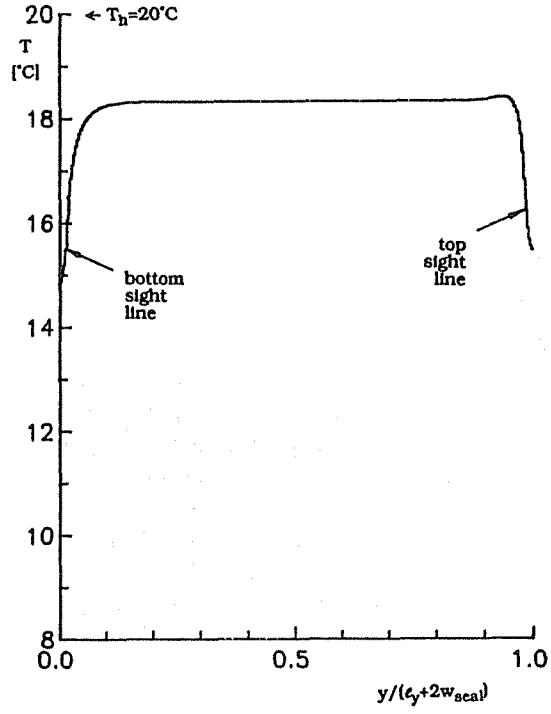

Figure 10 *Temperature distribution along vertical cut at hot cavity wall (unit 1).*

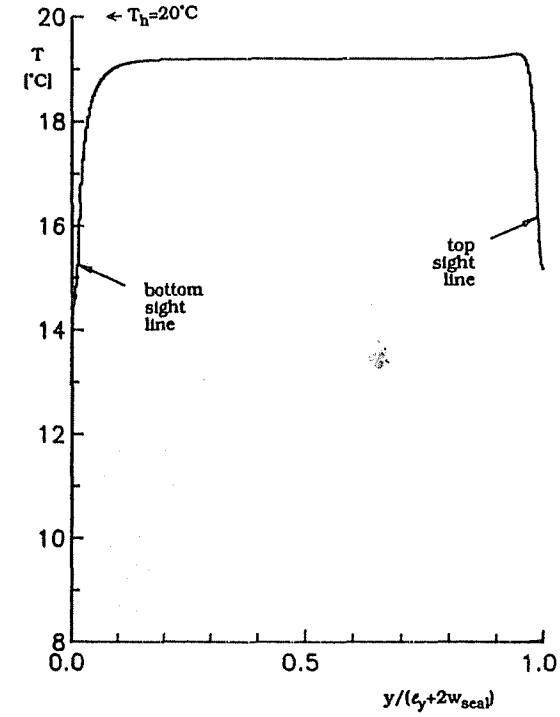

Figure 11 *Temperature distribution along vertical cut at hot cavity wall (unit 2).*

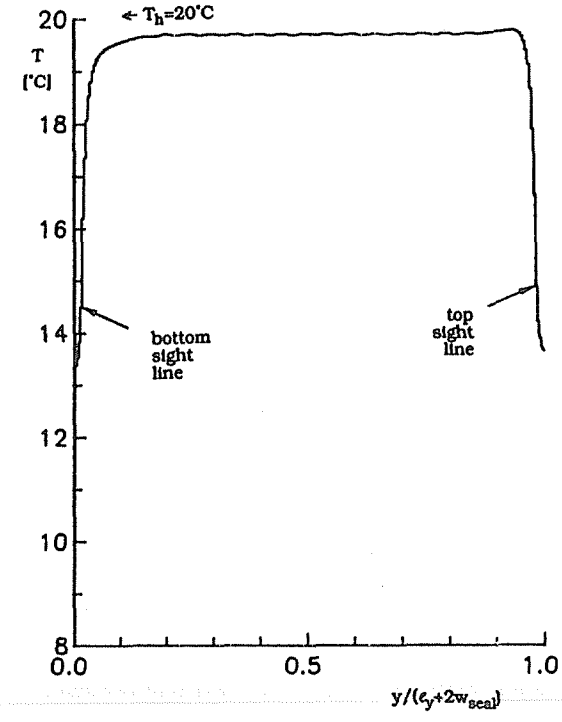

Figure 12 *Temperature distribution along vertical cut at hot cavity wall (unit 3).*

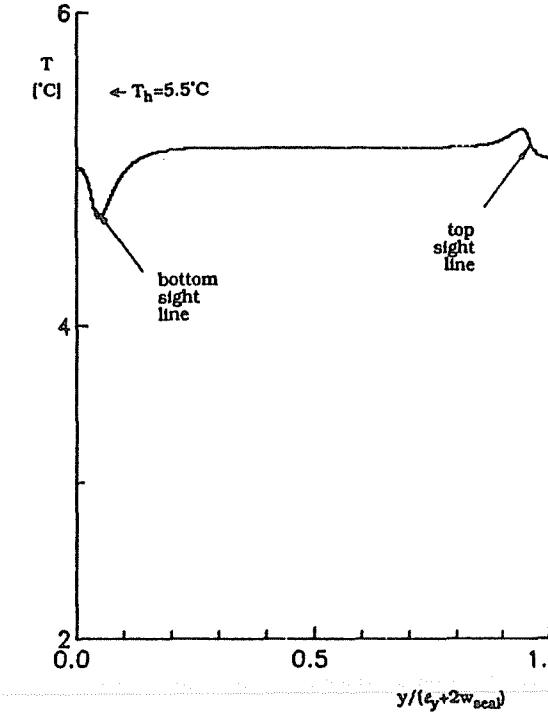

Figure 13 *Temperature distribution along vertical cut at hot cavity wall (unit 7).*

Guarded heater plate measurements have been found to agree well with calculated heat flux values for a number of glazing systems with a wide variety of glazing system and edge-seal components. Simulation results have provided insights regarding the heat flux patterns and temperature profiles inside these glazing systems. The importance of fill-gas motion in determining the minimum indoor pane temperature has been demonstrated.

ACKNOWLEDGMENTS

This research was supported by CANMET (Natural Resources Canada) and by the Natural Science and Engineering Research Council of Canada.

Guarded heater plate experiments were performed using the equipment of the Solar Thermal Research Laboratory (STRL) at the University of Waterloo. The assistance of Professor K.G.T. Hollands, by providing equipment and time for discussion, is appreciated.

REFERENCES

Bergholtz, R.F. 1978. Instability of steady natural convection in a vertical fluid layer. *Journal of Fluid Mechanics* 84(4): 743-768.

Hutchinson, B.R., and G.D. Raithby. 1986. A multigrid method based on the additive correction strategy. *Numerical Heat Transfer* 9: 511-537.

Patankar, S.V. 1980. *Numerical heat transfer and fluid flow.* New York: Hemisphere Publishing Corp.

Press, W.H., B.P. Flannery, S.A. Teukolsky, and W.T. Vetterling. 1986. *Numerical recipes: The art of scientific computing.* Cambridge: Cambridge University Press.

Siegel, R., and J.R. Howell. 1972. *Thermal radiation heat transfer.* New York: McGraw-Hill.

Sparrow, E.M., and R.D. Cess. 1976. *Radiation heat transfer*, augmented ed. New York: McGraw-Hill.

Vandoormaal, J.P., and G.D. Raithby. 1984. Enhancements of the SIMPLE method. *Numerical Heat Transfer* 7: 147-163.

Wright, J.L. 1989. Thermal resistance measurement of glazing system edge-seals. Second National Conference on Energy Efficient Cooling, Bethesda, MD.

Wright, J.L. 1990. The measurement and computer simulation of heat transfer in glazing systems. Ph.D. thesis, Mechanical Engineering Department. Waterloo, ON: University of Waterloo.

Wright, J.L., and H.F. Sullivan. 1987a. Simulation and measurement of windows with low emissivity coatings used in conjunction with Teflon inner glazings. *ISES Solar World Congress*, Hamburg, West Germany, vol. 4, pp. 3136-3140.

Wright, J.L., and H.F. Sullivan. 1987b. Simulation and measurement of windows with metal films used in conjunction with Teflon inner glazings. *International Conference on Building Energy Management*, Lausanne, Switzerland, vol. 4, pp. 5-12.

Wright, J.L., and H.F. Sullivan. 1988. Glazing system U-value measurement using a guarded heater plate apparatus. *ASHRAE Transactions* 94(2).

Wright, J.L., and H.F. Sullivan. 1989a. Natural convection in sealed glazing units: A review. *ASHRAE Transactions* 95(1).

Wright, J.L., and H.F. Sullivan. 1989b. Thermal resistance measurement of glazing system edge-seals and seal materials using a guarded heater plate apparatus. *ASHRAE Transactions* 95(2).

Wright, J.L., and H.F. Sullivan. 1994. A 2-D numerical model for natural convection in a vertical, rectangular window cavity. *ASHRAE Transactions* 100(2).